
VARX GRANGER ANALYSIS: MODELING, INFERENCE, AND APPLICATIONS

Lucas C Parra
Biomedical Engineering
City College of New York
parra@ccny.cuny.edu

Aimar Silvan
Biomedical Engineering
City College of New York
asilvanortubay@ccny.cuny.edu

Maximilian Nentwich
The Feinstein Institutes for Medical Research
Northwell Health
max.nentwich@gmail.com

Jens Madsen
Biomedical Engineering
City College of New York
madsen@ccny.cuny.edu

Behdash Babadi
Electrical and Computer Engineering
University of Maryland
behtash@umd.edu

ABSTRACT

Vector Autoregressive models with exogenous input (VARX) provide a powerful framework for modeling complex dynamical systems like brains, markets, or societies. Their simplicity allows us to uncover linear effects between endogenous and exogenous variables. The Granger formalism is naturally suited for VARX models, but the connection between the two is not widely understood. We aim to bridge this gap by providing both the basic equations and easy-to-use code. We first explain how the Granger formalism can be combined with a VARX model using deviance as a test statistic. We also present a bias correction for the deviance in the case of L2 regularization, a technique used to reduce model complexity. To address the challenge of modeling long responses, we propose the use of basis functions, which further reduce parameter complexity. We demonstrate that p-values are correctly estimated, even for short signals where regularization influences the results. Additionally, we analyze the model's performance under various scenarios where model assumptions are violated, such as missing variables or indirect observations of the underlying dynamics. Finally, we showcase the practical utility of our approach by applying it to real-world data from neuroscience, physiology, and sociology. To facilitate its adoption, we make Matlab, Python, and R code available here: <https://github.com/lcparra/varx>

1 Introduction

The Granger formalism relies on temporal precedence to establish the direction of effects: It tests whether the linear prediction of a variable $y(t)$ from its past can be improved by adding the history of another variable $x(t)$ as predictor [1]. If it does, we say that x has an "effect" on y .¹ This basic idea had originally been proposed by Wiener [2] leading to the term "Wiener-Granger Causality" [3]. For multiple variables, this linear prediction naturally fits in the formalism of vectorial autoregressive (VAR) models [4]. The VAR-Granger formalism is appealing to neuroscientists, economists, and sociologists because it allows one to quantify the strength and direction of effects in interactive dynamical systems, such as brains [3, 5], markets [6], and societies [7]. When such systems are subject to an external stimulus, the appropriate model is a VAR model with eXogenous input – the VARX model.

¹In this work we avoid calling the effect "causal", as there are too many caveats to this interpretation; see Discussion.

Exogenous variables were incorporated into the Granger formalism as conditional dependence by Geweke [8]. In practice, this "conditional causality" has been used to control for spurious correlations due to common causes. Code implementations of this idea [9, 10] only use exogenous variables to remove confounds. In contrast, we propose to model the total system response as a combination of both exogenous effects and endogenous dynamics. In this view, the exogenous effects are not a nuisance, but an important component of the model to be estimated, encompassing multiple time delays. Although economists have employed VARX models to capture exogenous effects, the use of the Granger formalism to establish the effects of individual variables is not as widely used. Indeed, the correspondence of the "conditional Granger-causality" [3, 11] with VARX models is not well known. While the VARX model is common in statistics toolboxes, we are not aware of any implementation of the VARX model with the Granger-Geweke test to assess the effects.

Here we apply the Granger-Geweke formalism in the language of VARX models, capturing both internal dynamics and exogenous inputs. We summarize the basic equations needed to estimate model parameters, effect size, and statistical significance. To cope with high-dimensional datasets and longer prediction filters, we use L2 regularization and basis functions, effectively reducing the number of parameters. Notably, we derive the de-biased estimates for L2 regularization for the first time. We also illustrate instances where interpreting the Granger formalism as 'causal' may be misleading, such as in cases of missing variables or colliders. We offer examples showcasing the application of this formalism to neural signals, highlighting the differences between the VARX models and "temporal response functions" [12] often used in neuroscience. We also show examples with physiological and sociological data. Finally, we close with a discussion on the specifics of implementation in code, and some caveats on the interpretation of model results.

2 Methods

2.1 VARX model

Consider the vectorial "input" signal $\mathbf{x}(t)$ and the vectorial "output" signal $\mathbf{y}(t)$ of dimensions d_x and d_y respectively, with both assumed to be observable (lower-case bold characters represent vectors). In the present context, the input may be multiple features of a continuous natural stimulus, say luminance and sound volume of a movie. The output could be neural activity recorded at multiple locations in the brain. The simplest model we can envision is one where the current signal $\mathbf{y}(t)$ can be predicted linearly from the input $\mathbf{x}(t)$ and also linearly from the preceding output $\mathbf{y}(t-1)$.

$$\mathbf{y}(t) = \mathbf{A} * \mathbf{y}(t-1) + \mathbf{B} * \mathbf{x}(t) + \mathbf{e}(t), \quad (1)$$

where \mathbf{A} and \mathbf{B} are filter matrices of dimensions $[d_y, d_y]$ and $[d_y, d_x]$, with filters of length n_a and n_b , respectively. The additive term $\mathbf{e}(t)$ represents an unobserved "innovation" that introduces an error in the prediction. In linear systems it is called innovation because it injects novelty into the recurrent dynamic. Here we have used a compact formulation of a multi-input multi-output convolution, which for the auto-regressive and moving average filters reads:

$$\mathbf{A} * \mathbf{y}(t-1) = \sum_{l=1}^{n_a} \mathbf{A}(l) \cdot \mathbf{y}(t-l), \quad (2)$$

$$\mathbf{B} * \mathbf{x}(t) = \sum_{l=0}^{n_b-1} \mathbf{B}(l) \cdot \mathbf{x}(t-l). \quad (3)$$

Equation (1) is called a VARX model or "equation error" model [13]. It is different from an "output error" model where the recursion has no error, but the recursive signal $\mathbf{z}(t)$ is hidden and only observed with additive noise (see Fig. 1):

$$\begin{aligned} \mathbf{z}(t) &= \mathbf{A} * \mathbf{z}(t-1) + \mathbf{B} * \mathbf{x}(t), \\ \mathbf{y}(t) &= \mathbf{z}(t) + \mathbf{e}(t). \end{aligned} \quad (4)$$

Note that in both cases the total response of the dynamical system (the impulse response) can be written in the Z or Fourier domains simply as

$$\mathcal{H} = \mathcal{Y}\mathcal{X}^{-1} = (\mathbf{I} - \mathcal{A})^{-1}\mathcal{B}. \quad (5)$$

where cursive upper-case corresponds to transform-domain variables. In this view, what we are proposing is to model the total system response as a combination of a Moving Average (MA) filters \mathbf{B} and Auto-Regressive (AR) filters $(\mathbf{I} - \mathbf{A})^{-1}$. In the time domain, the total system response can be simply computed by passing impulses in each input variable through the systems, while setting the error/innovation to zero, $\mathbf{e}(t) = 0$.

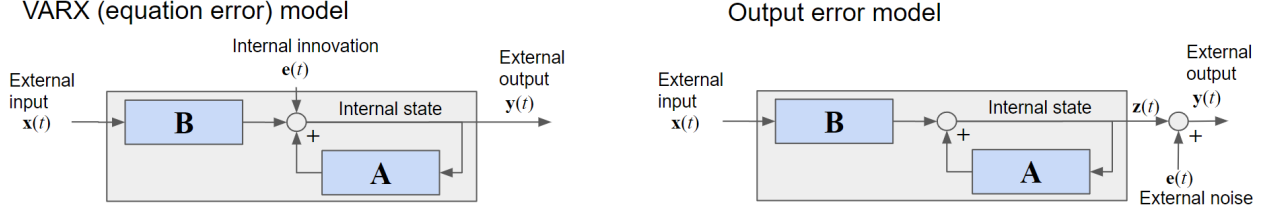


Figure 1: Model schematic: In the output error model the internal state is not observable. The gray box represents the overall system response \mathcal{H} .

Given observed $\mathbf{x}(t), \mathbf{y}(t)$ one can estimate the parameters \mathbf{A} and \mathbf{B} by minimizing the mean of square error:

$$\sigma^2 = \frac{1}{T} \sum_{t=1}^{\mathcal{X}} e^2(t). \quad (6)$$

For zero-mean signals this is also the variance, hence the conventional symbol σ^2 , which is vectorial here as it is computed and minimized for each dimension in \mathbf{y} individually. For the equation error or VARX model, the linear predictors $\mathbf{y}(t-1)$ and $\mathbf{x}(t)$ are observable, and parameter estimation results in a simple linear least-squares problem with a well-established closed form solution. Equation (1) can be rewritten as

$$\mathbf{Y} = \mathbf{X} \cdot \mathbf{H} + \mathbf{E}, \quad (7)$$

where \mathbf{X} is a block-Toeplitz matrix of the predictors with dimensions $[T, N]$. Here N is the total number of free parameters for each predicted dimension in $\mathbf{y}(t)$, i.e. $N = d_y n_a + d_x n_b$, \mathbf{Y} is the output signal $\mathbf{y}(t)$ arranged as a matrix of dimensions $[T, d_y n_a]$, and $\mathbf{H} = [\mathbf{A}, \mathbf{B}]^\top$ is a matrix of dimensions $[d_y n_a, N]$ combining the AR and MA filters. The least-squares estimate is then simply:

$$\hat{\mathbf{H}} = \mathbf{R}_{xx}^{-1} \mathbf{R}_{xy}. \quad (8)$$

Matrices \mathbf{R}_{xx} and \mathbf{R}_{xy} are block-toeplitz capturing cross-correlations:

$$\mathbf{R}_{xx} = \mathbf{X}^\top \cdot \mathbf{X}, \quad (9)$$

$$\mathbf{R}_{xy} = \mathbf{X}^\top \cdot \mathbf{Y}. \quad (10)$$

The estimated output is:

$$\hat{\mathbf{Y}} = \mathbf{X} * \hat{\mathbf{H}}. \quad (11)$$

The residual errors of this model prediction for each output channel are the diagonal elements of the correlation matrix for the errors:

$$\mathbf{R}_{ee} = (\mathbf{Y} - \hat{\mathbf{Y}})^\top \cdot (\mathbf{Y} - \hat{\mathbf{Y}}) = \hat{\mathbf{H}}^\top \cdot \mathbf{R}_{xx} \cdot \hat{\mathbf{H}} - 2\hat{\mathbf{H}}^\top \cdot \mathbf{R}_{xy} + \mathbf{R}_{yy}, \quad (12)$$

$$\sigma^2 = \frac{1}{T} \text{diag}(\mathbf{R}_{ee}). \quad (13)$$

For the output error model, the square error is not a quadratic function of the parameters \mathbf{A} and \mathbf{B} , and a few different iterative optimization approaches have been proposed, such as an expectation maximization (EM) algorithm [14], gradient back-propagation through time [15, 16], or “pseudo regression” [13]. The pros and cons of the equation-error versus the output-error models are elaborated in the Discussion section.

Note that Equations (2)-(11) are identical in the “temporal response function” (TRF) formalism [12], whereby matrix \mathbf{X} only contains the input \mathbf{x} and with $N = d_x n_b$, and the impulse response \mathbf{H} is then called a multivariate TRF.

2.2 Granger formalism

To establish if any of the channels in filters \mathbf{A} and \mathbf{B} significantly improve predictions – i.e. have an “effect” – one can use a likelihood-ratio test [17]. In this formalism, one uses deviance as the test statistics to quantify the contribution of a given predictor in \mathbf{X} for each output in \mathbf{Y} . The approach consists of estimating filter parameters \mathbf{H} for \mathbf{X} intact, which is referred to as the “full” model, and then again with one of the predictors removed, which is referred to as the

“reduced” model. We compute the resulting square error $\hat{\sigma}_f^2$ and $\hat{\sigma}_r^2$, for the full and reduced models, and obtain the *deviance* between the two models as test statistics (there is one deviance value for each dimension in \mathbf{y}):

$$\mathcal{D} := T \log \hat{\sigma}_r^2 / \hat{\sigma}_f^2, \quad (14)$$

where the division of the two variance vectors and the log operator are interpreted element-wise. For normal, independent, and identically distributed error, the vector \mathcal{D} contains the log-likelihood ratios (times a factor of 2), with each element following a chi-square distribution [18]. Notice that the test statistics vector \mathcal{D} is formed by computing the log-likelihood ratio for each output dimension, and for each predictor dimension that is removed in the reduced model. Thus, one can estimate the statistical significance of each channel in \mathbf{A} and \mathbf{B} by computing the full model once, and then removing each predictor variable individually from the full model. The statistical significance for a non-zero contribution from a particular predictor to a particular output is then given by an element of the “p-value” vector computed with the corresponding deviance vector:

$$\mathbf{p} = \mathbf{1} - F(\mathcal{D}, n), \quad (15)$$

Here F is the cumulative distribution function for the chi-square distribution and n is the number of parameters that were removed in the reduced model, i.e. n_a or n_b depending if an element of $\mathbf{y}(t-1)$ or $\mathbf{x}(t)$ was removed. The operation of F on a vector is interpreted element-wise.

2.3 Debiased Deviance for L2 Regularization

To avoid overtraining on small sample sizes, i.e. where T is not much larger than N , we decided to use an L2 penalty, with Tikhonov regularization. The advantage over other forms of regularization, such as L1 [19, 20] or a state space model [10, 10] is computational efficiency thanks to the closed-form solution:

$$\hat{\mathbf{H}} = (\mathbf{R}_{xx} + \gamma \mathbf{\Gamma})^{-1} \mathbf{R}_{xy}, \quad (16)$$

where we selected $\mathbf{\Gamma} = \text{diag}(\mathbf{R}_{xx})$ so that all variables are regularized equally regardless of their scale. The choice of γ is discussed in the results section. This regularization introduces (purposefully) a bias in the estimate, and the deviance estimate has to be corrected to account for this bias [21]. The term that corrects the log-likelihood in case of L2 regularization is (derived in the Appendix):

$$\mathbf{b} = \frac{1}{2} \text{diag}(\mathbf{R}_{xe}^\top \cdot \mathbf{R}_{xx}^{-1} \cdot \mathbf{R}_{xe}) / \text{diag}(\mathbf{R}_{ee}), \quad (17)$$

where the division between the two diagonal vectors is element-wise and $\mathbf{R}_{xe} = \mathbf{R}_{xy} - \mathbf{R}_{xx} \cdot \hat{\mathbf{H}}$. This bias term has to be computed for the full and reduced models, giving \mathbf{b}_f and \mathbf{b}_r respectively. The corresponding de-biased deviance is then:

$$\mathcal{D}^{de-biased} = T \log \hat{\sigma}_r^2 / \hat{\sigma}_f^2 - \mathbf{b}_r + \mathbf{b}_f, \quad (18)$$

and can be used to compute the p-values as before. We have found empirically that we obtain a better (conservative) estimate of p-values if we use $T' = T - N$ instead of T in this calculation of the de-biased deviance. T' represents the effective degrees of freedom of the full model and converges to T in the asymptotic limit for which the de-biased deviance formula was derived.

2.4 Effect size

Note that deviance increases linearly with T , that is, the statistical evidence increases with the length of the signals. The actual benefit of adding a link to the model is given by the log-ratio of the residual variances, and that remains constant with increasing signal duration. This log-ratio can be seen as a measure of effect size. Regularization can make this log-ratio negative and this is what the bias terms correct for. In this work, we take $\mathcal{D}^{de-biased} / T$ as a metric of effect size (e.g. in Fig. 9). A traditional definition of effect size in the context of reduced and full linear models is the coefficient of determination, or generalized R-square [22]:

$$R^2 := \mathbf{1} - \exp -\mathcal{D}^{de-biased} / T, \quad (19)$$

where the exponential of a vector is interpreted element-wise.

2.5 Basis functions for the moving average filters

The filter length (number of parameters) used in AR filters is typically kept relatively short, to avoid over-fitting, reduce the odds of instability in the recursion, and because even a single delay can already represent an infinite impulse response. This is not the case for MA filters, where longer responses have to be modeled explicitly, resulting in a

relatively large number of parameters, with a risk of over-fitting. We have found empirically that the corrections we introduced in the Deviance estimate for short signals (Eq. 18) do not work well when the filter lengths for \mathbf{A} and \mathbf{B} are very different. A solution to both these problems (imbalance in number of parameters and filter length) is to use basis functions for the \mathbf{B} filters, following an approach used previously for TRFs [23, 24, 25]. In this formalism, we have:

$$\mathbf{B} = \underline{\mathbf{B}} \circ \mathbf{W}, \quad (20)$$

where the inner product \circ is along the lag-axis of the filter matrix \mathbf{B} , and the goal now is to find the optimal $\underline{\mathbf{B}}$. The matrix \mathbf{W} has dimensions $[n_b, \underline{n}]$ so that the number of parameters per filter is reduced from n_b to \underline{n} . The linear least-squares problem remains unchanged with the closed-form solutions using now $\underline{\mathbf{X}} = \mathbf{W}\mathbf{X}$. In the equations above this can be implemented by replacing \mathbf{R}_{xx} and \mathbf{R}_{xy} with:

$$\mathbf{R}_{xx} = \mathbf{W} \circ \mathbf{R}_{xx} \circ \mathbf{W}^\top, \quad (21)$$

$$\mathbf{R}_{xy} = \mathbf{W} \circ \mathbf{R}_{xy}. \quad (22)$$

Note that the new \mathbf{R}_{xx} and \mathbf{R}_{xy} are no longer Toeplitz matrices. The Granger formalism applies without change.

Here we implemented Gaussian windows as shown in Figure 5A. With this, we are not only reducing the number of parameters, i.e. regularizing the solutions, but also selecting among a set of smooth filters \mathbf{B} .

3 Results

Details on all results provided next can be found in the accompanying code repository <https://github.com/lcparra/varx>.

3.1 Test of model estimation on known model

To validate the estimation algorithm and code, we simulated a simple VARX model with two outputs and one input ($d_y = 2, d_x = 1$). The algorithm correctly recovers the AR and MA parameters (Fig.2). VARX model estimation is available as part of the econometric toolbox in Matlab, but is limited to instantaneous input $n_b = 1$, i.e. no filtering of the input. When limiting the simulation to this case, the algorithms obtain similar results. Small variations are expected based on how the initial conditions (boundaries) are handled and numerical differences. In our implementation we omit from the estimate all samples that do not have a valid history. The code handles missing values (NaN) in the same way.

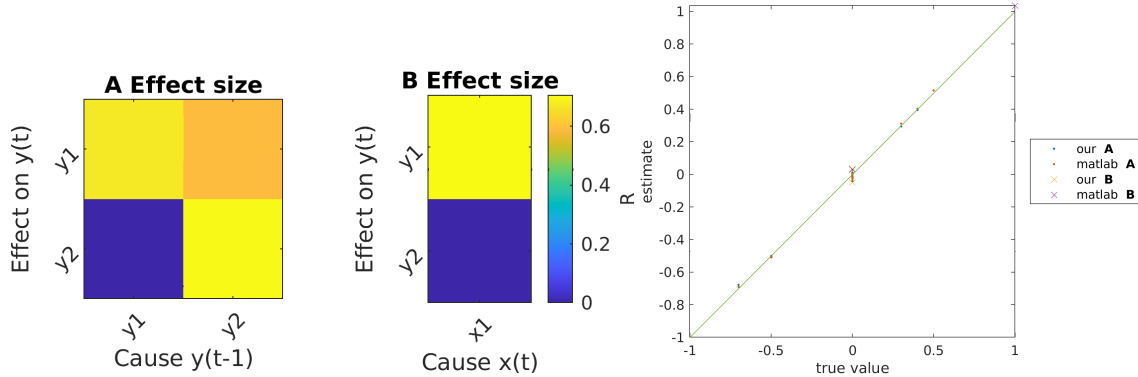


Figure 2: Comparison of estimated parameters to true parameters in a simple toy example. Here $x_1 \rightarrow y_2$ and $y_1 \rightarrow y_2$ were zero in the simulated data. In this simulation signals are generated with i.i.d innovation. We used $T = 1000, \lambda = 0$ and $n_a = 3, n_b = 1$ in both simulation and estimation.

3.2 Validation of p-values

To determine if the estimation computes correct p -values we simulated and VARX model with some channels set to zero, and others with non-zero values. We did this with a small and large simulated dataset, generated with normal i.i.d. innovations. We repeat the simulation 1000 times and determine how many times the zero channels report a $p < 0.05$. We find a false discovery rate of approximately 0.05 for that specific null-channel, suggesting that p -values are correctly estimated (Fig. 3).

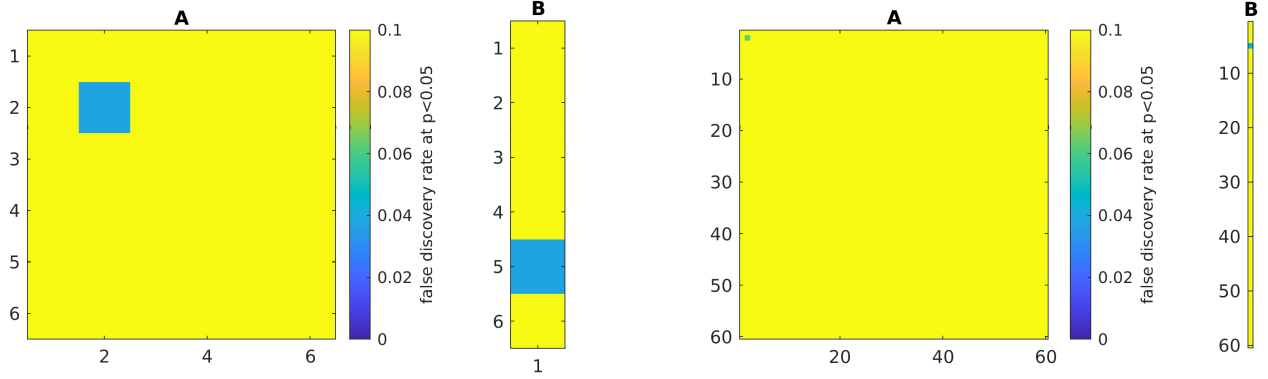


Figure 3: Validation of p -values in both a small and a larger model ($d_y = 6$ and $d_y = 60$). Significance is set of $p < 0.05$, so we expect a false discovery rate of 0.05. Simulation here used with $d_x = 1, n_a = 2, n_b = 2, T = 1000, \lambda = 0.0$. Filter coefficients for **B** were selected at random from unit variance normal, and **A** values were set to be ± 0.05 with sign selected at random (this insured stable recursion in practice). Only two links are set to zero $A(:, 2, 2) = 0, B(:, 5, 1) = 0$, for these two, the p -value is correctly estimated at approximately 0.05 (green).

3.3 Validation of p -values with L2 regularization

As T increases the need for regularization decreases, so we scale the regularization factor as $\gamma = \lambda / \sqrt{df}$, where λ is a choice of regulation in the order of 1. This particular scaling was established empirically to accomplish two things. One, if γ is kept large for large T , then the asymptotic approximation used to compute the de-biased deviance is no longer correct and p -values are miss-estimated. Second, the specific scaling with the square root is an empirical finding that places the optimal γ at similar values of λ in simulation with different signal lengths T . In Fig. 4 we simulated a simple model for varying λ and T . In this example we find, as expected, that training error increases with regularization (Fig. 4a), but test error decreases with increasing regularization (Fig. 4b). This effect becomes clear with larger noise (note that the explained variance here is relatively small) and with increasing correlation in input (here random normal inputs were drawn independently). The second observation is that with increasing sample size T , test error drops, and regularization becomes less important. Finally, we see that the bias correction provides conservative control of the false discovery rate (Fig. 4c). The expected value in this example is 0.05 and at small T we are well below that. Indeed, for small T we seem to be over-correcting, which limits the power to detect a true effect Fig. 4d).

3.4 Example of using basis functions

For large T there is minimal regularization and regularization can not be used to “smooth” the estimated filters. For that, we developed the basis functions decomposition using smooth basis functions. A second motivation was also to make the number of parameters of **A** and **B** filters comparable, as we noticed empirically that an imbalance results in quite skewed p -values. We simulated examples with very different filter lengths $n_a = 2, n_b = 60, n = 6$ (Fig. 5). We find that introducing basis functions improves the estimates of false discovery rate while providing smooth filter estimates. We noticed empirically that these basis functions, for slow signals, made the signals significantly larger in power. As a result, conventional ridge regression regularized different signals differently, resulting in a miss-estimation of values. This motivated the adoption of Tikhonov regularization so that all variables are regularized by the same amount.

3.5 Example: Intracranial recordings in human

In our view, one of the main advantages of a VARX model is the factorization of the overall system response into an AR and MA portion, which separates the effect of the endogenous variables into an initial response that then reverberates in the recurrence of the dynamical system. To demonstrate this we analyze an example of an intracranial EEG recording in a 49-year-old male patient, included in [26]. The patient watched a total of 43.6 minutes of movie clips while recording iEEG and eyetracking. We focus on a subset of 50 electrodes covering visual brain areas, including the occipital cortex, fusiform face area and parahippocampal cortex. The neural data was preprocessed as described in [26] before extracting high-frequency broadband power (70-150Hz and downsampled to 60Hz). The exogenous “input” is a pulse train indicating the start of fixations, i.e. the moments when the subject receives new visual input. What is most evident is that the **B** response is shorter than the full impulse response **H**. When estimating it directly or as $\mathbf{H} = (\mathbf{I} - \mathbf{A})^{-1}\mathbf{B}$ we see that the two are very similar. This suggests that the VARX model decomposes the total response into a fast

VARX GRANGER ANALYSIS

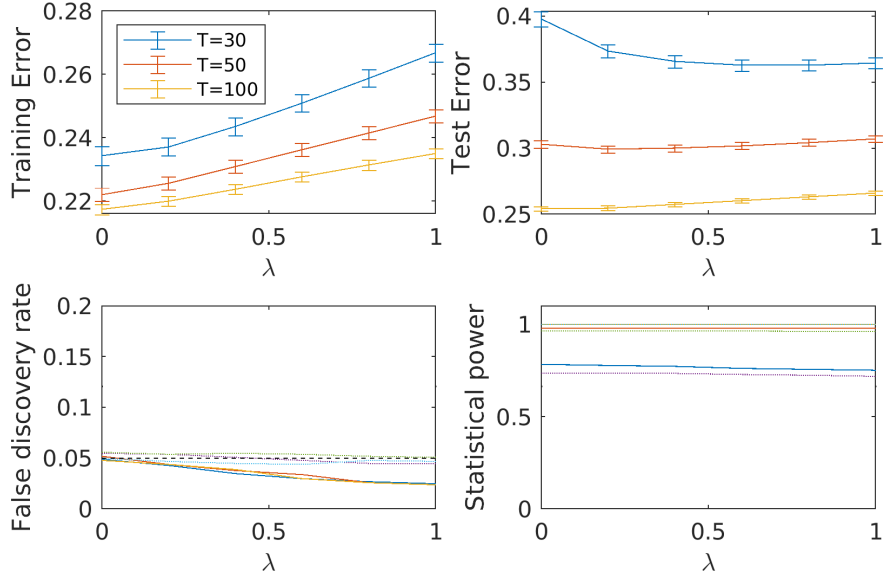


Figure 4: Effect of L2 regularization on small toy examples $d_y = 2, d_x = 2$. We ran the model and fit the data computing analysis of p-values in 1000 simulations with normal distributed error (zero mean, std of 2) and inputs x (zero mean, std of 1). (a) the training error is the relative error, i.e. $\sigma_e^2 / \text{std}(y)^2$ computed on the same data that the model was fit on (length T samples). Error bars indicate SEM over the 1000 simulations. (b) test error is the same relative error but computed on newly simulated data with the estimated model. (c) False discovery is the fraction of times where the null path is $p < 0.05$. Solid lines are for false discovery in **A**, and dotted lines are for false discovery in **B** in this simulation. (d) Statistical power is the fraction of times that the $p > 0.05$ for the path that has non-zero coefficients. The specific models tested here had effects of $y_1 \rightarrow y_2$ and $x_2 \rightarrow y_2$ set to zero and otherwise $n_a = 2, n_b = 10$ coefficients with non-zero values.

response followed by a prolonged response due to the recurrence in the brain network. The VARX model appears to be therefore a valid factorization of the full system response estimated traditionally.

3.6 Example: Physiological signals in human

Another dynamical system is the body, with multiple interconnected signals such as respiration, heart, pupil, and brain. Here we are analyzing data from [27] which showed bidirectional effects for several of these signals during various controlled conditions. We estimated a VARX model for this data suggesting possible directional effects between various physiological variables (Fig. 7). Pupil size and heart rate were measured in the experiment as they are conventional metrics of physiological arousal. As variables are added to the VARX model the connectivity structure is typically preserved. In this specific example using the controlled breathing task, we initially observe a bidirectional link between pupil size and heart rate, however this disappears once respiration is taken into account. Instead, it is explained by an effect of respiration on pupil size, together with the well-established bidirectional link between respiration and heart rate that is recovered in this data. The effect of saccades on pupil identified here is also well established. In general, adding variables can remove links – if the addition is a common cause, or add links – if the addition is a "collider". This is well established for i.i.d samples [28], and is no different for temporally correlated time sequence data.

3.7 Example: Sociology

As a final example, we present an analysis from the area of sociology. Here we analyze the history of union participation, and how it relates to strikes (Fig. 8A). The hypothesis we want to test is if strikes increase union membership in subsequent years. We assume that the unemployment rate can not be influenced by any of the union variables. It therefore is modeled as an exogenous input variable, whereas the number of workers in unions and on strike, as well as the number of strikes, can in principle all affect each other. VARX Granger analysis suggests (Fig. 8B) suggests that unemployment affects unionization, which in turn affects number of strikes, which obviously affects the number of workers on strike. These results depended on the choice of parameters n_a, n_b, λ . Only the effect of NumberOfStrikes

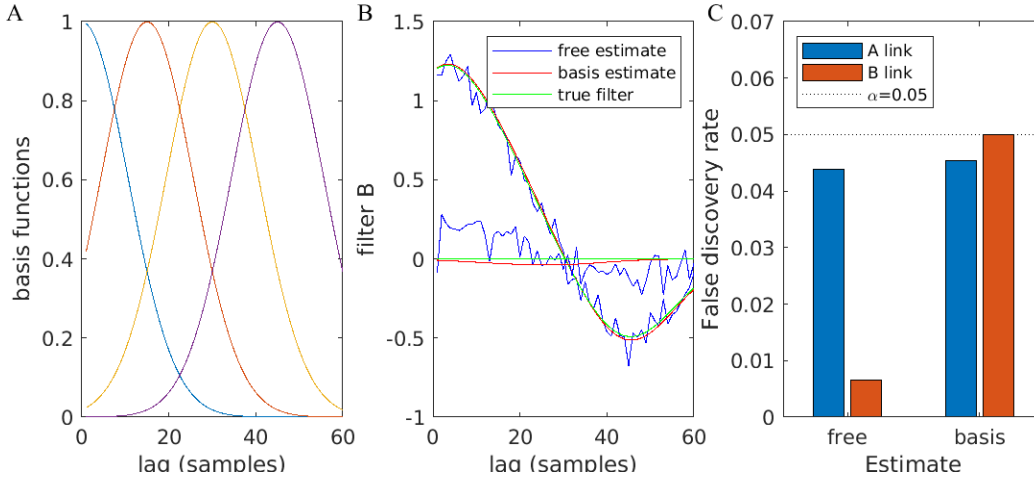


Figure 5: Estimate MA filter coefficients \mathbf{B} with and without basis functions (basis vs free, respectively). (A) The Gaussian basis functions used here, both for the generation of the data and for estimation. (B) Corresponding filter estimates and true filters used during data generation. Here $d_y = 2$ and $d_x = 1$, with $y_1 \rightarrow y_2$ and $x \rightarrow y_2$ channels set to zero. Data was simulated with $T = 300$ and $n_a = 3$, $n_b = 60$, $n_{bar} = 4$. The total number of free parameters was $4 * n_a + 2 * n_b = 132$ (free) and $4 * n_a + 2 * n_b = 20$ (basis). No regularization was used. (C) False discovery rate for AR and MA channels with and without basis functions. False discovery (bars) indicates how many times in 5000 random simulations these missing links reported a $p < 0.05$, therefore we expect discovery rate to be 0.05 (dotted line).

→ WorkersOnStrike was robust to parameter choice. What did not robustly emerge from this data is evidence for the initial hypothesis that strikes lead to an increase in union participation.

3.8 The case of a missing and superfluous variable

Finally, we wanted to evaluate the case where the model does not match the data generation process. We simulated three possible data generation processes with one input and two outputs ($d_x = 1, d_y = 2$). We simulated three cases, where the exogenous input x (conditioning variable) will be either a common cause, a collider, or an independent variable (see Figure 9). In all cases, the simulation implements a one-directional effect $y_1 \rightarrow y_2$. We then measure how frequently we find $p < 0.05$ for this path, i.e. the power of the test to identify a correct path, and how frequently we find $p < 0.05$ for $y_1 \leftarrow y_2$, i.e. the rate of false discovery. Note that conditioning on a collider is known to introduce spurious correlations [28]. We test this for data generated with both the equation (VARX) and output error models. The results in Figure 9 indicate the false discovery rate is correctly estimated at 0.05 in most scenarios, i.e. we are not finding causal effects above chance where there were none. This result holds regardless of whether x was included as input (i.e. as a control variable with instant or delayed effect) or whether it did or did not have a true effect on y_1 and y_2 (common cause vs independent). Only when incorrectly modeling a collider as input, did we obtain spurious effects. Statistical power was improved when including the input to the model. In summary, there is no risk of false discovery when including input variables, even if they don't have a true effect, except if they are actually affected by the internal variables y .

Despite using the VARX model, when the data was generated with an output error model, the false discovery remains limited at the target of 0.05. However, a common unobserved cause can generate spurious effects $y_1 \leftarrow y_2$. It has been suggested that running a Granger causality model on time-reversed data provides a control for this situation [29, 30]. We have found that running the model on time-reversed data results in spurious effects in all conditions tested here, so it is not clear to us how this can provide a remedy, and the caveat of an unobserved common cause remains when we are not directly observing endogenous variables, but only a noisy version of the internal dynamic.

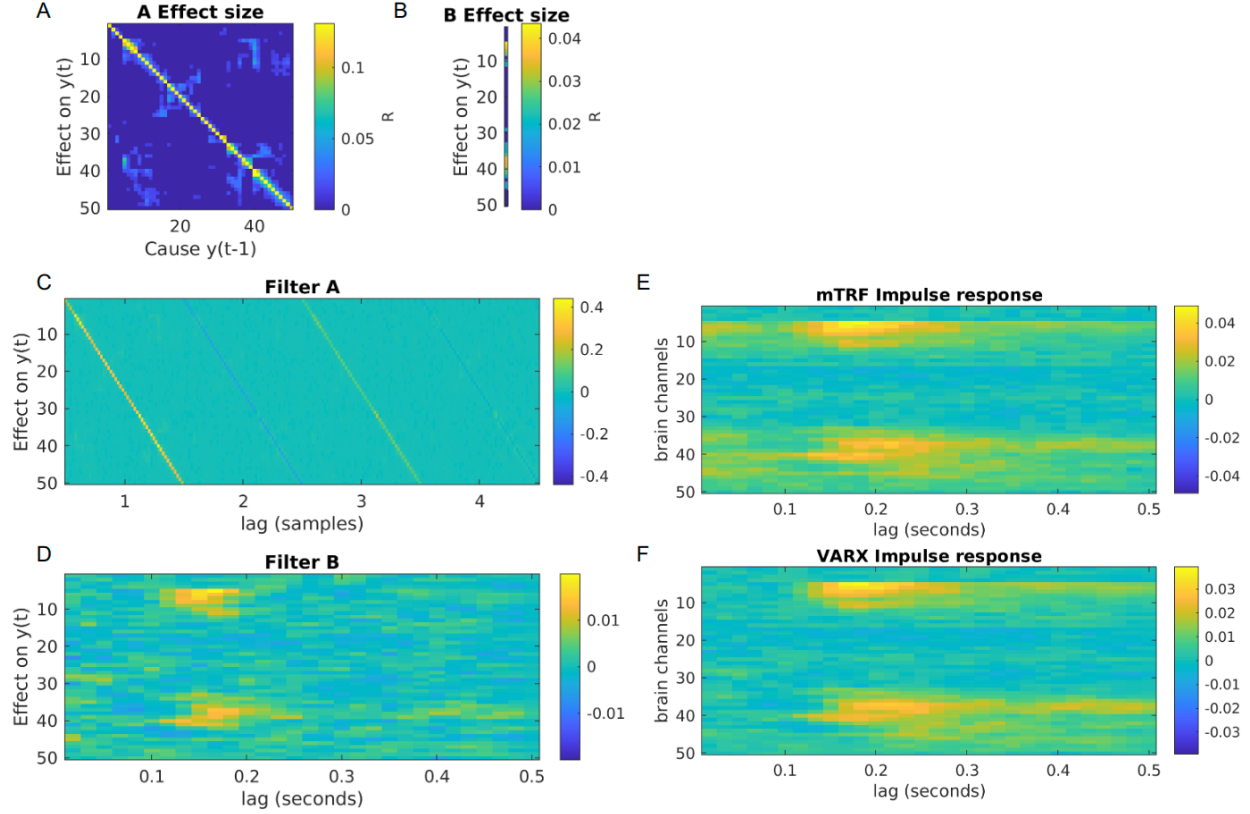


Figure 6: Example of intracranial recording in humans. Here a VARX model is fit to Broad-band high-frequency activity during free viewing of 7 videos recorded in ($d_y = 50$) electrodes. A total of 43.6 minutes of data were used at a sampling rate of 60Hz ($T = 156, 955$) from a single patient. (A) Effect size R for the recurrent connectivity **A** between recording electrodes – in the language of neuroscience, this could be called "functional connectivity". (B) Effect size R of fixation onset as exogenous variable on different electrodes. (C) **A** filter coefficients ($n_a = 4$). Diagonal terms dominate. (D) **B** filter coefficients $n_b = 30, \underline{n} = 20, \lambda = 0$. (E) System response estimated directly – in the language of neuroscience, this is the multivariate "temporal response function" (mTRF). (F) System response resulting from the VARX model estimate (Eq. 5). Data from [26].

4 Discussion

Equation error versus output error models

The estimation of model parameters for a VARX model has a closed-form solution, thus being much faster than finding parameters for an output error model, which requires iterative algorithms. The gain in computational efficiency results from the assumption that $y(t)$ is observable. This may not be a good assumption in the case of brain signals measured across the skull, such as EEG/MEG where only a linear mixture, possibly with added noise, is observed. In that case, iterative algorithms are needed, but the Granger formalism can still be used with some effort [20]. In the VARX model, however, we do not need to assume that all internal activity is directly observable. Any unobserved activity is captured as innovation $e(t)$. We only need to be aware that any recurrent connectivity may be due to those unobserved common "causes". In particular symmetric effect sizes R will be suggestive of such a missing variable. The role of the error is quite different in the two models. In the VARX (equation error) the error is an internal source of innovation driving the recurrent dynamic similar to the drive that comes from the input. The internal states are fully observable. In the output error model, the input entirely drives the system, and the error only affects the observations and is not injected into the dynamic.

VARX GRANGER ANALYSIS

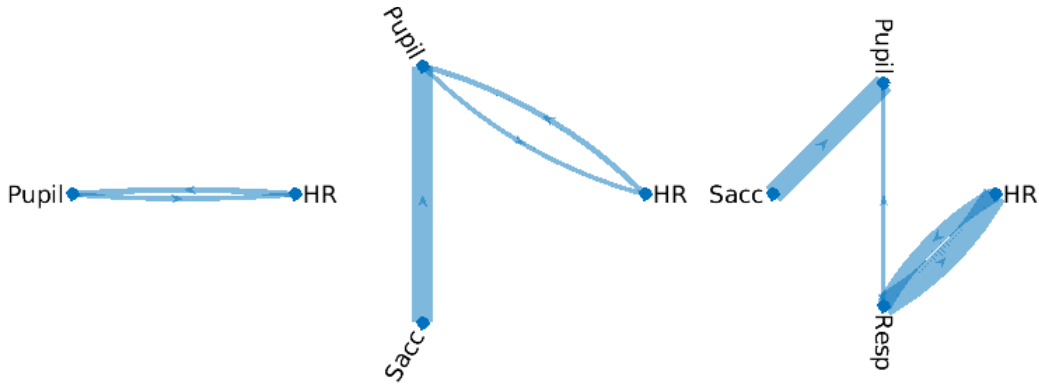


Figure 7: Example of physiological signals in human. This data was collected while people carried out a controlled breathing intervention. In this case there was no exogenous stimulus, so we only fit a VAR model. Links in **A** are show if $p < 0.001$. Here we had 26 minutes of data from compiled across multiple subjects samples at 25Hz ($T = 26 * 60 * 25$). Data from [27].

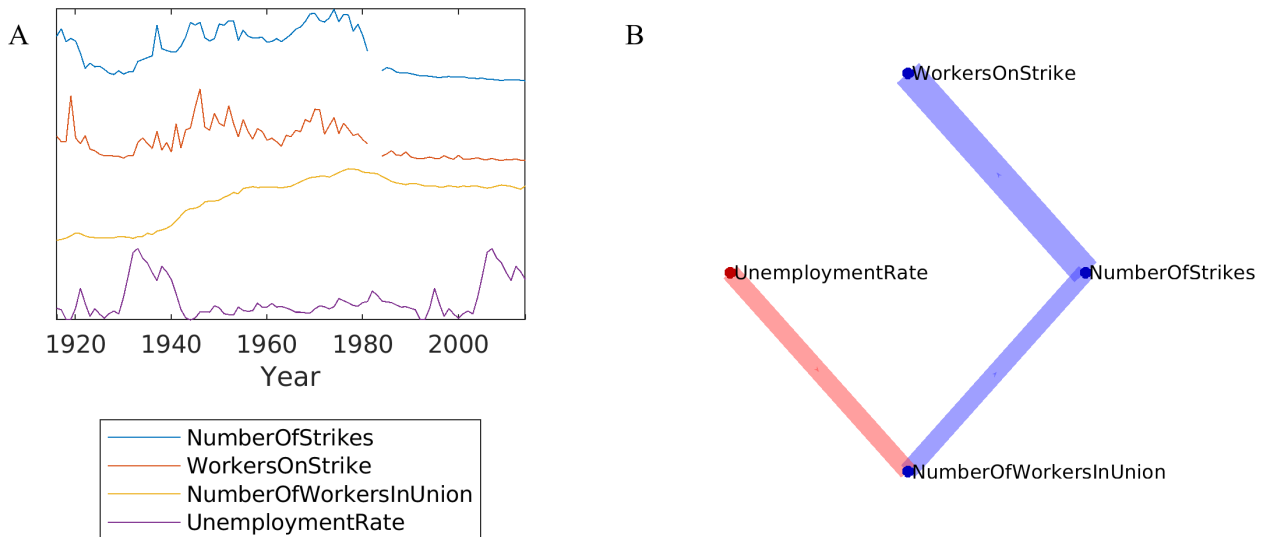


Figure 8: Example on union participation and strikes: (A) Historical data from the US. We treated the unemployment rate as an exogenous input in the VARX model, and the others as endogenous variables. (B) Significant effects in **A** and **B** are indicated in blue and red, respectively ($p < 0.05$, $n_a = n_b = 3$, $T = 91$, $\lambda = 0$). Note missing data around 1980, which was omitted during the estimation, including a 3-year history.

Sensitivity to parameters

A caveat to all results above is that individual links can be sensitive to the model assumptions, namely, which variables are selected as endogenous (and can be affected by all others), and which variables are selected as exogenous (and cannot be affected). An example of that was the choice of the unemployment rate as exogenous to the dynamic of unions. The results can also depend on which endogenous variables are included, as we saw in the example of physiological signals. Results can also depend on the number of parameters n_a and n_b and regularization factor λ (we saw this in the Union example). Although we did demonstrate this here, these parameters could be established with cross-validation.

Causality

In Granger's original formalism [1], the error of the full and reduced model refers to one-dimensional signals where $y(t - 1)$ is used in both cases and $x(t)$ is either used or omitted. If the error is significantly reduced by including $x(t)$ in the model, Granger argues that x "causes" y . This interpretation is inaccurate for several reasons [31]. As we saw,

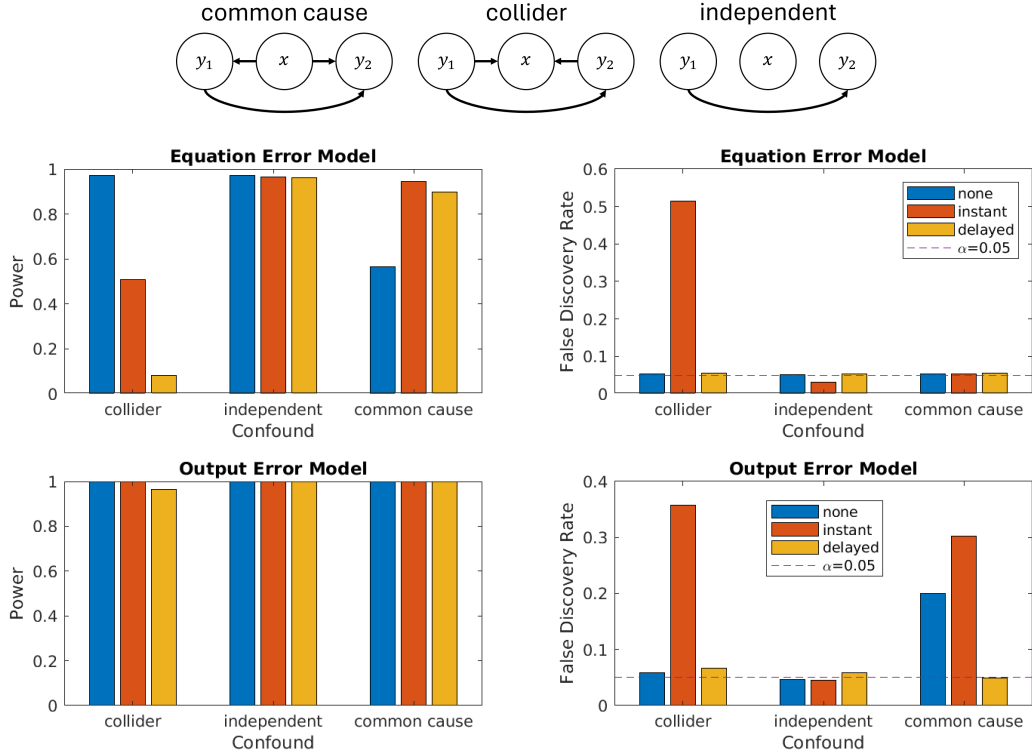


Figure 9: The VARX (equation error) model (1) requires a larger T to obtain similar power as the output error model (4). Simulation here used $n_a = n_b = 3, T = 5000$ and normal i.i.d. error.

when common causes are not observed (either as external input or internal variables) they can generate spurious links [32]. Similarly, including colliders can cause spurious links. All this is well explained by Pearl’s approach to causal inference [28]. Therefore one should not think of the Granger formalism as serious evidence for a causal graph without a well-justified prior graphical model [33]. In particular for large dimensional datasets such as brain data, where we only observe a tiny fraction of all the variables, the risk of unobserved common causes is much too large to take the resulting graph seriously as a causal graph. Nevertheless, asymmetries in the \mathbf{A} matrix can be seen as evidence of temporal precedence suggestive of an asymmetric "information flow".

Non-stationarity

Deviance makes a statistical judgment for the entire channel, not individual delays, as is common we simply treat each delay as a new predictor with its statistical test (this is the approach of the Matlab VARX). There are multiple methods under the umbrella of "Granger causality" that attempt to decide on how many tabs or which delays to use. By collapsing statistical evidence into a single test statistic, Deviance, this approach has greater statistical power. This is reflected in the linearity of D with the number of samples T . The flip side is that this statistic is very sensitive to violations of its assumptions. For instance, it assumes that all T samples of the innovation process are independent and identically distributed. The AR portion of the model assures that the linear-fit residual errors are uncorrelated in time, however, if there is any non-stationarity, this will no longer be the case. Therefore, non-stationarity will cause spurious correlations [34]. In particular, any transient will cause larger deflection and correlation across samples. In particular, transient that affect several signals, say a common edge at the start or end of the signal may appear to behave like a common drive with high amplitude that results in a spurious link. Therefore, in the present approach, one has to treat edges and transients with utmost care to avoid spurious links.

Some have argued that issues with non-linearity and non-stationarity can be addressed [35]. Barnett et al. proposed a State Space model that can cope to some degree with missing variables, does not need to compute a reduced model, and can deal with non-linearity and non-stationarity [35]. However, Stokes and Purdon showed that even the state-space Granger is not immune to confounding effects, non-stationarities, etc. The topic remains a matter of debate [36].

An alternative is to avoid using analytic expressions for the p -value, Eq. (15), and instead use standard non-parametric statistics. For time series, the simplest is to randomly time-delay channels relative to one-another, potentially with a circular wraparound. All else in the model identification, i.e. estimates \mathbf{A} , \mathbf{B} and effect size R^2 remain valid estimates of linear predictions even in the presence of non-stationarity and non-linearity.

Toolboxes

There are several software tools to estimate VARX models. We are not aware of one that provides the Granger-Geweke test for significance. The MVGC toolbox [10] does not report results on exogenous variables, <https://github.com/SacklerCentre/MVGC1>. Implementations of VARX models in Matlab Econometrics Toolbox and in SAS for instance, make significance statements for individual delays but do not allow for the exogenous variable, i.e. $nb = 1$. We welcome feedback if there other tools that that should be mentioned here. Our code emphasized computational efficiency to handle large datasets, with comparatively long \mathbf{B} filters.

Stability

A word about \mathbf{A} is in order. The AR filter $1/(1 - \mathbf{A})$ can be unstable. We have not implemented any mechanism for this vectorial AR filter to remain stable. Lack of stability only manifests in the systems when computing the overall systems response \mathbf{H} , which is not necessary during estimation for the \mathbf{B} , \mathbf{A} nor the calculation of statistical significance of each path (contrary to the output error model, where the recurrence has to be run back in time to estimated gradients, risking issues of stability (is this true?). We rarely encountered unstable AR estimates, and where we did, L2 regularization addressed the issues. But again, there is nothing in our formalism to ensure the stability of \mathbf{H} .

1/f spectrum

Another word about \mathbf{A} . The diagonal elements of \mathbf{A} in practice will always be high-pass filters, as we saw in the example of intra-cranial recordings. We advise not to take individual delays in the diagonal terms literally. The reason for this is that the innovation process is assumed to be white (constant spectrum), whereas all natural signals tend to have a 1/f spectrum. As a result, $1/(1 - \mathbf{A})$ has to have a 1/f spectrum, and \mathbf{A} has to scale with f , i.e. be high-pass. In practice, we find that this is entirely accomplished by the diagonal elements of \mathbf{A} . But the caveat in principle applies also to the off-diagonal elements. Future work could consider a VARMAX model where the innovation is first filtered and then injected into the recurrent dynamic [13]. However, estimation of VARMAX model parameters is a non-convex optimization problem with similar complications to the output-error model.

5 Conclusion

The "multivariate temporal response function" (TRF) approach for modeling the response of dynamical systems to exogenous variables essentially boils down to a vectorial MA model. And, unlike the VAR model, TRF is not commonly examined in the Granger formalism. Although Geweke introduced exogenous variables into the Granger formalism [8], the clear connection to the VARX model is not yet widely recognized. We hope to have bridged this gap. Different models vary in their assumptions about how to break down the system's overall response. When estimating with the VARX model, the data itself dictates how to factor the overall response into MA versus AR dynamics.

6 Acknowledgement

We would like to thank Vera E. Parra <veraeparra@gmail.com> for posing the question on union participation and compiling the corresponding datasets.

7 Appendix: Derivation of the De-biased Deviance

Consider the linear model in Eq. (7) for $n_y = 1$:

$$\mathbf{y} = \mathbf{X} \cdot \mathbf{h} + \mathbf{e}, \tag{23}$$

for simplicity of exposition. The case of $n_y > 1$ is a natural generalization, as we will explain below. A ridge regressor for \mathbf{h} is obtained by:

$$\hat{\mathbf{h}} := \underset{\mathbf{h}}{\operatorname{argmin}} \quad \|\mathbf{y} - \mathbf{X} \cdot \mathbf{h}\|^2 + \gamma \|\mathbf{h}\|^2, \tag{24}$$

where γ is the ridge parameter. To perform de-biasing, stationarity conditions for $\hat{\mathbf{h}}$ give:

$$-\mathbf{X}^\top(\mathbf{y} - \mathbf{X}\hat{\mathbf{h}}) + \lambda\hat{\mathbf{h}} = \mathbf{0}. \quad (25)$$

Following the arguments of Eqs. (3)–(5) in [37], the following estimator is the de-biased estimator:

$$\hat{\mathbf{h}}^{de-biased} = \hat{\mathbf{h}} + (\mathbf{X}^\top \mathbf{X})^{-1} \mathbf{X}^\top (\mathbf{y} - \mathbf{X}\hat{\mathbf{h}}) = \hat{\mathbf{h}} + \mathbf{R}_{xx}^{-1} \mathbf{r}_{xe}. \quad (26)$$

Now, consider the GC inference setting where we have full and reduce models given by:

$$\text{Full model: } \mathbf{y} = \mathbf{X}^f \mathbf{h}^f + \mathbf{e}^f, \quad \text{Reduced model: } \mathbf{y} = \mathbf{X}^r \mathbf{h}^r + \mathbf{e}^r. \quad (27)$$

The log-likelihoods of the full and reduced models are given by:

$$\ell^f := -\frac{T}{2} \ln(2\pi) - \frac{T}{2} \ln \sigma_f^2 - \frac{1}{2\sigma_f^2} \|\mathbf{y} - \mathbf{X}^f \mathbf{h}^f\|^2, \quad (28)$$

$$\ell^r := -\frac{T}{2} \ln(2\pi) - \frac{T}{2} \ln \sigma_r^2 - \frac{1}{2\sigma_r^2} \|\mathbf{y} - \mathbf{X}^r \mathbf{h}^r\|^2, \quad (29)$$

and the deviance difference is given by $\mathcal{D} := 2 \hat{\ell}^f - \hat{\ell}^r$, where $\hat{\ell}^f$ and $\hat{\ell}^r$ are, respectively, the full and reduced log-likelihoods evaluated at the ridge estimates of full and reduced parameters:

$$\hat{\mathbf{h}}^f := \underset{\mathbf{h}}{\operatorname{argmin}} \|\mathbf{y} - \mathbf{X}^f \mathbf{h}\|^2 + \lambda \|\mathbf{h}\|^2, \quad (30)$$

$$\hat{\mathbf{h}}^r := \underset{\mathbf{h}}{\operatorname{argmin}} \|\mathbf{y} - \mathbf{X}^r \mathbf{h}\|^2 + \lambda \|\mathbf{h}\|^2. \quad (31)$$

If the log-likelihoods were evaluated at the ML estimators, then \mathcal{D} would be asymptotically chi-square/non-central chi-square, allowing to perform precise statistical tests. But, the ridge estimator is different than the ML estimator. So, we need to de-bias the deviance difference.

Following Eq. (20) and Eqs. (B.2)–(B.6) in [20], the de-biased deviance difference is given by:

$$\mathcal{D}^{de-biased} = 2 \hat{\ell}^f - \hat{\ell}^r - B_r + B_f, \quad (32)$$

where the bias function $B(\cdot)$ is defined as:

$$b_f := \frac{1}{2\hat{\sigma}_f^2} \mathbf{y} - \mathbf{X}^f \hat{\mathbf{h}}^f \quad \mathbf{X}^f \mathbf{X}^{f\top} \mathbf{X}^f \quad \mathbf{X}^{f\top} \mathbf{X}^f \quad \mathbf{X}^f \mathbf{X}^{f\top} \quad \mathbf{X}^f \mathbf{X}^{f\top} \quad \mathbf{y} - \mathbf{X}^f \hat{\mathbf{h}}^f = \frac{1}{2r_{ee}^f} \mathbf{r}_{xe}^{f\top} \mathbf{R}_{xx}^f \mathbf{R}_{xx}^{f-1} \mathbf{r}_{xe}^f, \quad (33)$$

$$b_r := \frac{1}{2\hat{\sigma}_r^2} \mathbf{y} - \mathbf{X}^r \hat{\mathbf{h}}^r \quad \mathbf{X}^r \mathbf{X}^{r\top} \mathbf{X}^r \quad \mathbf{X}^{r\top} \mathbf{X}^r \quad \mathbf{X}^r \mathbf{X}^{r\top} \quad \mathbf{y} - \mathbf{X}^r \hat{\mathbf{h}}^r = \frac{1}{2r_{ee}^r} \mathbf{r}_{xe}^{r\top} \mathbf{R}_{xx}^r \mathbf{R}_{xx}^{r-1} \mathbf{r}_{xe}^r. \quad (34)$$

Simplifying the deviance difference \mathcal{D} for the linear model, we can express $\mathcal{D}^{de-biased}$ as:

$$\mathcal{D}^{de-biased} = T \ln \frac{\hat{\sigma}_r^2}{\hat{\sigma}_f^2} - b_r + b_f, \quad (35)$$

where

$$\hat{\sigma}_f^2 := \frac{1}{T} \|\mathbf{y} - \mathbf{X}^f \hat{\mathbf{h}}^f\|^2 = r_{ee}^f, \quad \hat{\sigma}_r^2 := \frac{1}{T} \|\mathbf{y} - \mathbf{X}^r \hat{\mathbf{h}}^r\|^2 = r_{ee}^r, \quad (36)$$

are the full and reduced prediction variances. For $n_y > 1$, given that each channel of \mathbf{Y} is treated separately, the full and reduced bias vectors are given by:

$$\mathbf{b}_f = \frac{1}{2} \operatorname{diag}(\mathbf{R}_{xe}^{f\top} \cdot \mathbf{R}_{xx}^f \mathbf{R}_{xx}^{f-1} \cdot \mathbf{R}_{xe}^f) / \operatorname{diag}(\mathbf{R}_{ee}^f), \quad \mathbf{b}_r = \frac{1}{2} \operatorname{diag}(\mathbf{R}_{xe}^{r\top} \cdot \mathbf{R}_{xx}^r \mathbf{R}_{xx}^{r-1} \cdot \mathbf{R}_{xe}^r) / \operatorname{diag}(\mathbf{R}_{ee}^r), \quad (37)$$

and the de-biased deviance vector is given by:

$$\mathcal{D}^{de-biased} = T \log \frac{\hat{\sigma}_r^2}{\hat{\sigma}_f^2} - \mathbf{b}_r + \mathbf{b}_f. \quad (38)$$

Under the null hypothesis, the de-biased deviance difference can be shown to be asymptotically, as $T \rightarrow \infty$, chi-square distributed with n degrees of freedom, where n is the number of parameters removed in the reduced model and T is the number of observations (i.e., column dimension of \mathbf{Y}) [18]. This asymptotic property requires that ridge estimator is consistent. To guarantee this, γ must grow slower than $\mathcal{O}(T)$. In practice, fixing γ using cross-validation typically guarantees this.

References

- [1] Clive WJ Granger. Investigating causal relations by econometric models and cross-spectral methods. *Econometrica: journal of the Econometric Society*, pages 424–438, 1969.
- [2] Norbert Wiener. The Theory of Prediction. In Edwin F. Beckenbach, editor, *Modern Mathematics of the Engineer: First series*, pages 165–190. Dover Publications, Inc., 1956.
- [3] Steven L Bressler and Anil K Seth. Wiener–granger causality: a well established methodology. *Neuroimage*, 58(2):323–329, 2011.
- [4] Ali Shojaie and Emily B Fox. Granger causality: A review and recent advances. *Annual Review of Statistics and Its Application*, 9:289–319, 2022.
- [5] Anil K Seth, Adam B Barrett, and Lionel Barnett. Granger causality analysis in neuroscience and neuroimaging. *Journal of Neuroscience*, 35(8):3293–3297, 2015.
- [6] Duo Qin. Rise of var modelling approach. *Journal of Economic Surveys*, 25(1):156–174, 2011.
- [7] John R Freeman. Granger causality and the times series analysis of political relationships. *American Journal of Political Science*, pages 327–358, 1983.
- [8] John F Geweke. Measures of conditional linear dependence and feedback between time series. *Journal of the American Statistical Association*, 79(388):907–915, 1984.
- [9] Shuixia Guo, Anil K Seth, Keith M Kendrick, Cong Zhou, and Jianfeng Feng. Partial granger causality—eliminating exogenous inputs and latent variables. *Journal of neuroscience methods*, 172(1):79–93, 2008.
- [10] Lionel Barnett and Anil K Seth. The MVGC multivariate granger causality toolbox: a new approach to granger-causal inference. *J. Neurosci. Methods*, 223:50–68, February 2014.
- [11] Mingzhou Ding, Yonghong Chen, and Steven L Bressler. Granger causality: basic theory and application to neuroscience. *Handbook of time series analysis: recent theoretical developments and applications*, pages 437–460, 2006.
- [12] Michael J Crosse, Giovanni M Di Liberto, Adam Bednar, and Edmund C Lalor. The multivariate temporal response function (mTRF) toolbox: A MATLAB toolbox for relating neural signals to continuous stimuli. *Front. Hum. Neurosci.*, 10:604, November 2016.
- [13] L Ljung. System identification-theory for the user 2nd edition ptr prentice-hall. *Upper Saddle River, NJ*, 1999.
- [14] R H Shumway and D S Stoffer. An approach to time series smoothing and forecasting using the em algorithm. *J. Time Ser. Anal.*, 3(4):253–264, July 1982.
- [15] J J Shynk. Adaptive IIR filtering. *IEEE ASSP Mag.*, 6(2):4–21, April 1989.
- [16] Carles Igual, Jorge Igual, Janne M Hahne, and Lucas C Parra. Adaptive auto-regressive proportional myoelectric control. *IEEE Transactions on Neural Systems and Rehabilitation Engineering*, 27(2):314–322, 2019.
- [17] John Geweke. Measurement of linear dependence and feedback between multiple time series. *J. Am. Stat. Assoc.*, 77(378):304–313, June 1982.
- [18] R R Davidson and W E Lever. The limiting distribution of the likelihood ratio statistic under a class of local alternatives. *Sankhyā Indian J. Stat. Ser.*, 32:209–224, 1961.
- [19] Proloy Das and Behtash Babadi. Non-asymptotic guarantees for reliable identification of granger causality via the LASSO. *IEEE Trans. Inf. Theory*, 69(11):7439–7460, November 2023.
- [20] Behrad Soleimani, Proloy Das, I M Dushyanthi Karunathilake, Stefanie E Kuchinsky, Jonathan Z Simon, and Behtash Babadi. NLGC: Network localized granger causality with application to MEG directional functional connectivity analysis. *Neuroimage*, 260(119496):119496, October 2022.
- [21] Alireza Sheikhattar, Sina Miran, Ji Liu, Jonathan B Fritz, Shihab A Shamma, Patrick O Kanold, and Behtash Babadi. Extracting neuronal functional network dynamics via adaptive granger causality analysis. *Proc. Natl. Acad. Sci. U. S. A.*, 115(17):E3869–E3878, April 2018.
- [22] Lonnie Magee. R2Measures based on wald and likelihood ratio joint significance tests. *Am. Stat.*, 44(3):250–253, August 1990.
- [23] Sahar Akram, Jonathan Z Simon, and Behtash Babadi. Dynamic estimation of the auditory temporal response function from MEG in competing-speaker environments. *IEEE Trans. Biomed. Eng.*, 64(8):1896–1905, August 2017.

- [24] Sina Miran, Sahar Akram, Alireza Sheikhattar, Jonathan Z Simon, Tao Zhang, and Behtash Babadi. Real-time tracking of selective auditory attention from M/EEG: A bayesian filtering approach. *Front. Neurosci.*, 12, May 2018.
- [25] I M Dushyanthi Karunathilake, Jason L Dunlap, Janani Perera, Alessandro Presacco, Lien Decruy, Samira Anderson, Stefanie E Kuchinsky, and Jonathan Z Simon. Effects of aging on cortical representations of continuous speech. *J. Neurophysiol.*, 129(6):1359–1377, June 2023.
- [26] Maximilian Nentwich, Marcin Leszczynski, Brian E Russ, Lukas Hirsch, Noah Markowitz, Kaustubh Sapru, Charles E Schroeder, Ashesh D Mehta, Stephan Bickel, and Lucas C Parra. Semantic novelty modulates neural responses to visual change across the human brain. *Nat. Commun.*, 14(1):2910, May 2023.
- [27] Jens Madsen and Lucas C Parra. Bidirectional brain-body interactions during natural story listening. *Cell Reports*, 43(4), 2024.
- [28] Judea Pearl. Linear models: A useful “microscope” for causal analysis. *J. Causal Inference*, 1(1):155–170, May 2013.
- [29] Martin Vinck, Lisanne Hurdeman, Conrado A Bosman, Pascal Fries, Francesco P Battaglia, Cyriel M A Pennartz, and Paul H Tiesinga. How to detect the granger-causal flow direction in the presence of additive noise? *Neuroimage*, 108:301–318, March 2015.
- [30] Irene Winkler, Danny Panknin, Daniel Bartz, Klaus-Robert Muller, and Stefan Haufe. Validity of time reversal for testing granger causality. *IEEE Trans. Signal Process.*, 64(11):2746–2760, June 2016.
- [31] Mariusz Maziarz. A review of the granger-causality fallacy. *The journal of philosophical economics: Reflections on economic and social issues*, 8(2):86–105, 2015.
- [32] Helmut Lütkepohl. Non-causality due to omitted variables. *Journal of econometrics*, 19(2-3):367–378, 1982.
- [33] J. Pearl. *Causality*. Causality: Models, Reasoning, and Inference. Cambridge University Press, 2009.
- [34] Clive WJ Granger and Paul Newbold. Spurious regressions in econometrics. *Journal of econometrics*, 2(2):111–120, 1974.
- [35] Lionel Barnett and Anil K Seth. Granger causality for state-space models. *Phys. Rev. E Stat. Nonlin. Soft Matter Phys.*, 91(4):040101, April 2015.
- [36] Lionel Barnett, Adam B Barrett, and Anil K Seth. Misunderstandings regarding the application of granger causality in neuroscience. *Proceedings of the National Academy of Sciences*, 115(29):E6676–E6677, 2018.
- [37] Sara van de Geer, Peter Bühlmann, Ya’acov Ritov, and Ruben Dezeure. On asymptotically optimal confidence regions and tests for high-dimensional models. *The Annals of Statistics*, 42(3):1166–1202, June 2014. Publisher: Institute of Mathematical Statistics.